Linking microscopic guest properties to macroscopic observables in clathrate hydrates: Guest–host hydrogen bonding

ARTICLE *in* THE JOURNAL OF CHEMICAL PHYSICS · JUNE 2009

Impact Factor: 2.95 · DOI: 10.1063/1.3124187 · Source: PubMed

3 AUTHORS, INCLUDING:

John A. Ripmeester
National Research Council Canada
714 PUBLICATIONS **15,661** CITATIONS

SEE PROFILE

Linking microscopic guest properties to macroscopic observables in clathrate hydrates: Guest-host hydrogen bonding

Saman Alavi, Robin Susilo, and John A. Ripmeester

Citation: J. Chem. Phys. **130**, 174501 (2009); doi: 10.1063/1.3124187
View online: http://dx.doi.org/10.1063/1.3124187
View Table of Contents: http://jcp.aip.org/resource/1/JCPSA6/v130/i17
Published by the AIP Publishing LLC.

Linking microscopic guest properties to macroscopic observables in clathrate hydrates: Guest-host hydrogen bonding

Saman Alavi,[a] Robin Susilo, and John A. Ripmeester
Steacie Institute for Molecular Sciences, National Research Council of Canada, Ottawa, Ontario K1A 0R6, Canada

(Received 27 January 2009; accepted 2 April 2009; published online 1 May 2009)

Molecular dynamics simulations are used to compare microscopic structures and guest dynamics to macroscopic properties in structure II clathrate hydrates with cyclopentane, tetrahydrofuran (THF), 1,3-dioxolane, tetrahydropyran (THP), and *p*-dioxane as guests. Significant differences are observed between structural parameters and rotational dynamics for the different guests. The simulations show the formation of guest-host hydrogen bonds between the ether oxygen atoms of THF and THP and the cage water hydrogen atoms of the clathrate but the absence of similar hydrogen bonds in the clathrate hydrates of the other guests on the time scale of the calculations. This guest-host hydrogen bonding leads to the formation of Bjerrum *L*-defects in the clathrate water lattice where two adjacent water molecules have no covalently bonded hydrogen atom between them. Unlike Bjerrum defects of ice lattices, these guest-induced *L*-defects are not accompanied by the formation of a *D*-defect at an adjacent site in the water lattice. At the simulation temperature of 200 K, the guest-water hydrogen bonds in the THF clathrate are short lived (lifetime less than 1 ps) but in the THP they are longer lived (a minimum of 100 ps). A van't Hoff plot for the probability of defect formation in THF as a function of temperature gives an activation barrier of ~8.3 kJ/mol for guest-host defect formation in the THF clathrate. The consequences of the defect formation on the thermal expansivity, isothermal compressibility, dipole-dipole correlation function, and mechanical stability of the clathrate are discussed. © *2009 American Institute of Physics*. [DOI: 10.1063/1.3124187]

I. INTRODUCTION

When considering properties of natural gas hydrates, often resort is taken to the use of model systems as these are easier to handle experimentally. This relies on the commonly held opinion that the macroscopic properties of clathrate hydrates are more or less independent of the nature of the guest molecule.[1] This is an incautious assertion at best, as, in fact, a microscopic understanding of the guest-host interactions and their effect on macroscopic properties is still far from complete. It has been known for some time that the nature of the guest molecules in clathrate hydrates does indeed affect the equilibrium and dynamic properties of clathrate phases.[2] Guest size,[3,4] polarity, and hydrogen bonding capability affect the unit cell volumes, clathrate formation rates, clathrate stability ranges, and guest-host dynamics.

Just about all small molecules with a hydrophobic moiety that fit into the cavities of a clathrate structure are able to stabilize a metastable empty hydrate lattice if a minimum number of cavities are occupied. Regarding the nature of the guest molecule, the one proviso appears to be that strong, specific interactions between a potential guest and water must be absent to give a stable hydrate lattice. This is a rather qualitative assertion, as some water-soluble guest species are able to form clathrates—e.g., tetrahydrofuran (THF), dioxanes, and acetone, yet other water soluble species are known to be strictly inhibitors of clathrate hydrate formation, e.g., methanol, acetonitrile, and ethylene glycol. This phenomenon has been described macroscopically in terms of thermodynamic concepts such as the activity of the hydrate-forming solution,[5] and has been used practically in characterizing inhibitors of hydrate formation in natural gas pipelines, but there is no molecular scale understanding of the water molecule-guest interaction in hydrates that sheds light on the relative stability of specific hydrates.

Another clue pointing to the importance of the nature of the guest molecule in the clathrate hydrates is the guest dependence of the water lattice dynamics as measured by dielectric and magnetic relaxation. For instance, the relaxation properties of the host water lattices in structure II (sII) clathrates have been studied for a variety of guest molecules of different composition and with different polarities.[2] The dielectric relaxation of the host water lattice and guest dynamic motions occur in widely different time and frequency domains. The cage rattling and guest rotational motions are much faster than the reorientational motions of the water molecules in the clathrate lattice but the water relaxation rates do depend on the nature and dynamics of the guest in a particular clathrate. Dipolar, hydrogen bonding guests such as THF, dimethylether, and acetone in sII clathrates have dielectric relaxation times [O(1 μs)] which are two orders of magnitude smaller than those for nonpolar or nonhydrogen bonding polar guests [O(10^2 μs)].[2,6] The corresponding activation energy for water molecule reorientation times are 28–38 kJ mol^{-1} for the polar guests and ~50 kJ mol^{-1} for the nonpolar guests and the relaxation rate for hydrates depends on the dipole moment of the guest molecule.

[a]Electronic mail: saman.alavi@nrc-cnrc.gc.ca.

Although this correlation between macroscopic properties is well known, the mechanism of water relaxation in the clathrates remains unknown. It has been suggested that the difference in relaxation times for the dipolar and nonpolar guests is related to the injection of Bjerrum defects into the lattice by the formation of hydrogen bonds between the guests and cage water molecules.[7] In simple hydrogen bonded water networks like the ices, these defects are formed when a water molecule reorients so that two adjacent water oxygen atoms have either two hydrogen atoms in between them (*D*-defect) or no hydrogen atoms between them (*L*-defect). In extended hydrogen bonded water networks, Bjerrum defects by necessity occur in pairs. Furthermore, the *D*- and *L*-defects are known to diffuse separately and can annihilate upon encountering an opposite defect in the lattice. From measurements of water dynamics, the activation energy for the propagation of Bjerrum defects in the THF clathrate was measured to be ~25 kJ mol^{-1}.[5,8] The same value was obtained from ^{1}H NMR relaxation for water reorientation.[9,10]

If the water relaxation in the solid hydrate is influenced by a guest-host interaction such as hydrogen bonding, the guest dynamics are also expected to be affected. The dynamics of the guest motions in clathrate cages can be probed by proton and deuterium NMR relaxation time measurements.[8–10] The ^{2}H spectra of TDF-H_2O sII clathrate shows that the motion of the TDF molecules in sII clathrate cages becomes isotropic at 250 K with a narrow pseudo-Voigt lineshape with Δ (full width at half maximum) of ~2 kHz. At low temperatures (~125 K) the lineshape is Gaussian and Δ of the TDF peak increases to about 20 kHz.[9,11] Due to the proton disorder in the clathrate structure and the resulting different cage configurations at low temperatures, THF guests in each cage experience slightly different environments and thus display a broad pseudo-Gaussian ^{2}H NMR lineshape rather than a doublet with sharp components as expected for a well-defined motional state. Proton NMR relaxation times, T_1, have been measured for THF in the sII clathrate.[8–10,12,13] At temperatures below 200 K, the relaxation times follow the standard form for nuclear magnetic dipolar interaction,[14]

$$\frac{1}{T_1} = C_S^2[j_{CD}(\omega_0) + 4j_{CD}(2\omega_0)], \tag{1}$$

where j_{CD} is the Cole–Davidson spectral density and C is a structural parameter. Above 200 K, water relaxation is slow, although both water molecule reorientation and diffusion contribute.[2,13]

In this work we attempt to connect the molecular-scale behavior of clathrates with a number of different guest molecules and link this to macroscopic observables such as water relaxation. We examine the guest dynamics of the sII THF, 1,3-dioxolane, tetrahydropyran (THP), and *p*-dioxane clathrate with molecular dynamics simulations and compare these results to the guest dynamics in the nonpolar cyclopentane (CP) sII clathrate hydrate. We have not considered the cyclohexane sII clathrate since this clathrate needs a "help gas" to stabilize it. The guests with the same ring size are isoelectronic and have similar masses, but have very different dipole moments and hydrogen bonding abilities. We show that the differences in behavior are due to the interplay of volume of the guest molecule, its dipole moment vector, the specific interactions of the ether oxygen in the heterocyclic, hydrogen bonding guests with the cage water molecules, and the absence of such interactions in the CP clathrate. The dynamics of these guests and their interactions with the cage water molecules are studied in this work. The effect of the guest species on the structure, thermal expansivity, and isothermal compressibility of the clathrate phase are determined. We will see that in the polar guests, the combination of the direction of the molecular dipole moment and the preferred orientation for hydrogen bonding of the guest ether oxygen leads to the formation of either transient (THF) or long-lived (THP) guest-host hydrogen bonds and defects in the clathrate water lattice. The nature and frequency of the guest-host hydrogen bond formation are studied and connections to water relaxation dynamics in the clathrate phase are discussed. The water relaxation in clathrates is a slow process which occurs on a microsecond time scale and although there appears to be a clear connection between the ability to inject defects and the stability of the hydrate lattice, direct molecular dynamics simulation of this process is presently not possible.

Our molecular dynamics simulation methods are presented next. Microscopic structure, guest-host hydrogen bond formation, and guest dynamics of the clathrates in the large sII cages and the effect of the guest on the equilibrium thermodynamic properties of the clathrate phases are discussed afterwards. This paper ends with a discussion and conclusion.

II. MOLECULAR DYNAMICS METHODS

The initial coordinates of the water oxygen atoms in the sII clathrate cubic unit cell (a=17.0 Å) were taken from clathrate x-ray crystallography.[15] The O−H bond lengths are fixed at 1.0 Å and the initial positions of the water hydrogen atoms about the oxygen atoms were chosen to be consistent with the ice rules[16] while simultaneously minimizing the total dipole moment of the sII unit cell. The cubic simulation cells consisted of $2\times2\times2$ replicas of the unit cell with 1088 water molecules. The center of mass of each cyclic guest molecule was initially placed in the center of the large cages and the guest positions were allowed to equilibrate during the simulation. Further description of structure features of the sII unit cell and large cages are given in Ref. 5 and the supporting information.[17]

The intermolecular van der Waals potentials between atoms i and j on different molecules are considered to be the sum of Lennard-Jones (LJ) and electrostatic point charges,

$$V(r_i,r_j) = \sum_{i,j} 4\varepsilon_{ij}\left[\left(\frac{\sigma_{ij}}{r_{ij}}\right)^{12} - \left(\frac{\sigma_{ij}}{r_{ij}}\right)^{6}\right] + V_{q_1q_2}, \tag{2}$$

where σ_{ij} and ε_{ij} are the distance and energy parameters of the ij pair separated by a distance of r_{ij} and q_i and q_j are the electrostatic point charges on the atoms. Water molecules of the clathrate were modeled using the extended simple point charge model (SPC/E),[18] while the guest molecules were

TABLE I. Atomic point charges and LJ parameters for H_2O and selected atoms on guest molecules. The dipole moments of the guest molecules are also given. AMBER labels are used to specify atom types.

Atom	$q(e)$	μ(D)	ε_{ii}(kJ mol^{-1})	σ_{ii}(Å)
OW	−0.8476		0.650 2	3.1660
HW	+0.4238		0.0	0.0
OS (THF)	−0.4670	1.8109	0.711 28	3.0000
OS (THP)	−0.4926	1.6325		
OS (1,3-dioxolane)	−0.4736	1.7122		
OS (*p*-dioxane)	−0.4195	0		
C (CP)	+0.0316	0	0.457 73	3.3996
H1			0.065 69	2.4714
HC			0.065 69	2.6496

modeled with the general AMBER force field.[19] The values for the parameters σ_{ii} and ε_{ii} for selected atom types are given in Table I. Potentials between unlike atoms are calculated using the standard combination rules, $\varepsilon_{ij}=(\varepsilon_{ii}\varepsilon_{jj})^{1/2}$ and $\sigma_{ij}=(\sigma_{ii}+\sigma_{jj})/2$. Partial electrostatic charges on the atoms of the guest molecules were determined from charges from electrostatic potential grid (CHELPG) calculations[20] with the GAUSSIAN 98 suite of programs[21] at the B3LYP/6-311++G(d,p) level of theory. The point charges q_i on the water and ring oxygen atoms, along with the calculated dipole moment for the optimized guest molecules are given in Table I. The complete set of guest point charges are given in the supporting information.[17] This choice of force field for the clathrate and guests gives good estimates for the lattice vectors and other experimental data available in the equilibrated clathrates.[22,23]

Isotropic constant pressure/temperature *NpT* molecular dynamics simulations on periodic simulation cells were performed using the DL_POLY software program version 2.16.[24] The pressure was regulated using the modified Nosé–Hoover barostat algorithm[25] with thermostat and barostat relaxation times of 0.1 and 1.0 ps, respectively. The equations of motion were integrated with the Verlet leapfrog algorithm using a time step of 1 fs. Long-range electrostatic interactions were calculated using the Ewald summation method[26] with a precision of 1×10^{-6} and all intermolecular interactions in the simulation box were calculated within a cutoff distance of $R_{\text{cutoff}}=13.0$ Å. All simulations were performed for a total time of 150 ps, with the first 50 ps used for temperature scaled equilibration. Dynamics calculations at each temperature and pressure were performed starting with the final *NpT* configurations of the previous stage. Constant energy/volume *NVE* simulations for the dynamics were performed for a total of 250 ps with an equilibration time of 50 ps. Structural and dynamics parameters were extracted from the run times. Temperatures in the range of 100–250 K at ambient pressure were studied for each clathrate. Pressures from 0.01 to 5 kbar were considered at 250 K.

It should be noted that the SPC/E potential for water underestimates the melting point of the I_h ice phase[27] and the lattice constants of the clathrate phases (see below). For a detailed quantitative comparison of simulation results with experimental values, we would need to scale the nominal MD temperature values of the clathrate simulations to account for the difference in predicted and experimental melting points. The qualitative predictions of the SPC/E model are helpful in explaining the behaviors of the different experimental trends observed in the sII clathrate hydrated discussed below.

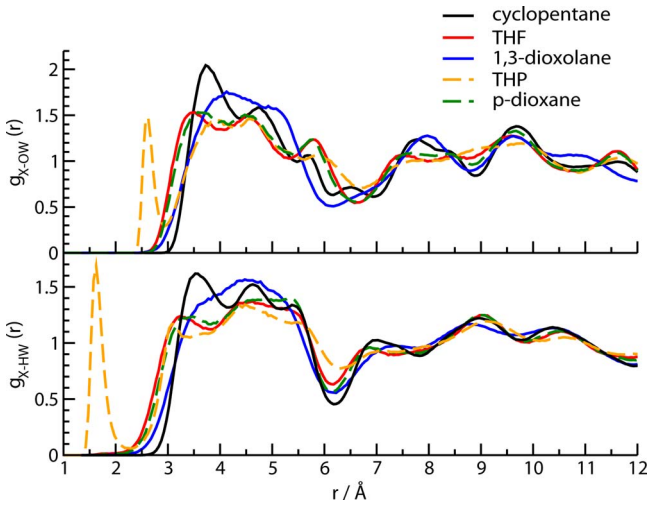

FIG. 1. (Color online) The RDF for chosen atoms (X) on the cyclic guests with the lattice water oxygen atoms (OW) and hydrogen atoms (HW). For the ethers, the chosen atom is the ether oxygen (OS) and for cyclopentane, the atom is an arbitrarily chosen carbon atom. Due to attractive electrostatic interactions, the first X-HW peaks are spaced inwards compared to the X-OW peaks. The first peaks in the OS-HW and OS-OW RDF of THP give a strong indication of hydrogen bonding between the oxygen in this ether with the water.

To study the formation of guest-host hydrogen bonds, the $28=(5\times12+6\times4)/3$ water molecules of the sII $5^{12}6^4$ large cages were labeled and at 0.25 ps intervals in the *NVE* trajectory, the distance of the ether oxygen atoms (OS) were measured with respect to all protons of the cage waters. If a OS-HW distance was less than 2.1 Å, a guest-host hydrogen bond was assumed to have formed and a "hit" assigned to the guest at that instant. The total lifetime of each guest-host hydrogen bond was recorded and the average probability of hydrogen bond formation in the simulation cell was determined at each temperature by averaging the ratio of times during the trajectory that all guest molecules spent hydrogen bonded to the cage water molecules. A similar procedure was carried out for CP which has no ether oxygen. A specific carbon atom of the ring was chosen to detect close ring-water contacts.

The dynamics of the rattling motions and rotations of the guests in the clathrate cages were also extracted from the *NVE* simulations. These properties can be related to experimentally determined NMR relaxation times.

III. RESULTS AND DISCUSSION

A. Structure and guest-host hydrogen bond formation

The radial distribution functions (RDFs) for the guest oxygen atoms (OS) of the cyclic ethers and a selected carbon atom of cyclopentane with the cage water oxygen (OW) and hydrogen (HW) atoms are shown in Fig. 1. The RDF plots show that the THF OS atoms have shorter average OS-OW and OS-HW distances than the corresponding CX distances

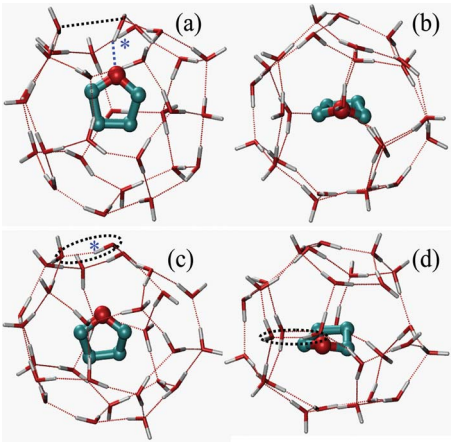

FIG. 2. (Color online) Snapshots of a large sII clathrate cage with a THF guest molecule at 200 K. (a) A THF-water hydrogen bond is indicated with the light dashed line and the asterisk. The guest-induced *L*-type Bjerrum defect formed between adjacent water molecules in the cage lattice is shown with the black dashed line. (b) The same configuration as part (a) seen from above. (c) A snapshot of the same sII clathrate large cage 0.25 ps after the configuration of part (a). The guest-host hydrogen bond has broken and the water molecule rotates back into position in the clathrate water lattice (shown with the ellipse), thus eliminating the *L*-type defect. (d) The same configuration as part (c) seen from above.

in CP. Moreover, as expected, the OS atoms interact at shorter distances with the HW atoms than with the cage OW atoms. The THP OS atoms have shorter OS-OW and OS-HW distances than the corresponding distances in the six-member ring *p*-dioxane. Of particular note are the short peak distances in the RDFs of THP where the average OS-HW and OS-OW distances are ~1.6, and ~2.5 Å, respectively. These bond lengths are within the range of normal hydrogen bonding.

Closer inspection of the molecular configurations of the guests in the large cages of THF and THP sII clathrates, as shown in Figs. 2 and 3, indicates the formation of guest-host hydrogen bonds and guest-induced defects in the hydrogen bonded water network of the large cages. In an ideal clathrate lattice, all of the water molecules are hydrogen bonded

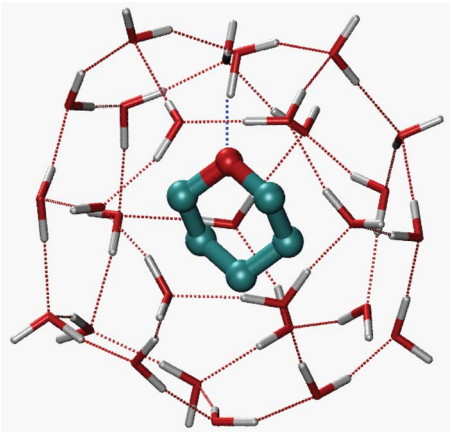

FIG. 3. (Color online) A snapshot of the sII large cage with a THP molecule at 200 K. The guest-host hydrogen bond is shown with the light dashed line. In the case of the THP clathrate, the guest-host hydrogen bonds are long lived and the *L*-type Bjerrum defects in the clathrate water lattice have a longer lifetime.

to other water molecules and there are no dangling OH bonds (see Fig. S2). Guest-host hydrogen bonds are formed as a result of the rotation of a water molecule in the lattice and hydrogen bonding of this water molecule to the ether oxygen of the THF and THP guests. Control simulations show that such water rearrangements do not occur without the presence of guests with electronegative atoms, see below. The guest-water hydrogen bonding leads to the formation of Bjerrum *L*-defects in the clathrate hydrogen bonding network near the large cage, where two oxygen atoms of adjacent water molecules have no hydrogen atom in between them. Unlike the Bjerrum defects in ice structures, the guest-induced *L*-defects are not accompanied by the formation of *D*-defects. During the lifetime of the *L*-defects, the clathrate faces which have the defect in their sides are distorted. Hydrogen bonding tethers the guests to the cage and reduces the mobilities of the THF and THP molecules. For the THF clathrate, the cage structure before and after the relaxation of the water into its lattice positions are shown in Fig. 2. The guest-host hydrogen bond is shown with the light dashed line and star in Fig. 2(a) and the *L*-defect between the oxygen atoms in the clathrate water hydrogen bonding network is shown by the black dashed line in Figs. 2(a) and 2(b). In the THF clathrate, the guest-host hydrogen bond and guest-induced defects have short lifetimes and the water molecule detaches from the THF oxygen and relaxes back into the lattice position as shown in two views in Figs. 2(c) and 2(d).

For the case of the THP clathrate shown in Fig. 3, the guest-host hydrogen bond formed in the large cages are much longer lived. For a 200 ps simulation trajectory, we observed that the guest OS is hydrogen bonded to a cage water molecule for an overwhelming majority of the time. In the snapshot shown, the *L*-defect in the lattice has migrated from its original position of formation.

The frequency and lifetimes of defect formation were studied at different THF and THP sII clathrate simulation temperatures. At higher temperatures, the range of the water lattice vibrations increases, and we observe that the number of guest-host hydrogen bonds formed in the THF clathrates increases. To quantify the formation of the defects, we considered 250 ps trajectories for the simulation cell. All configurations with the OS···H−OH distance less than 2.1 Å were considered to be hydrogen bonded and assigned a number 1 and other configuration assigned a number 0. Similar distance criteria have been used previously to characterize hydrogen bonding.[28] Hydrogen bond formation in a selected THF clathrate large cages at different times on the simulation trajectory at 200 and 250 K are shown in Fig. 4. Snapshots of the trajectory were taken at 0.25 ps intervals from the trajectory and hydrogen bond formation events were studied for 15 large cages in the simulation cell.

For the THF clathrate at 200 K, the lifetimes of the guest-host hydrogen bonding and the resulting lattice *L*-type Bjerrum defects are short and in most cases $\leq$0.25 ps sampling interval of the trajectory, see Fig. 4. An average lifetime for the guest-host hydrogen bonds, $\langle t \rangle$, can be obtained from

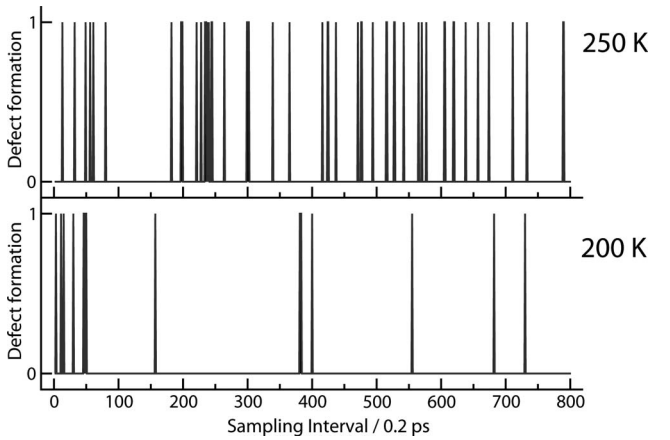

FIG. 4. Guest-host hydrogen bond formation for a selected THF sII clathrate large cages from a simulation trajectories at 250 K (top) and 200 K (bottom). Configurations with a guest-host hydrogen bond are shown with a number 1 and configurations with no such bonding are shown with a 0. At the higher temperature, hydrogen bond formation occurs much more frequently. The lifetimes of the hydrogen bonds are short at both temperatures.

$$\langle t \rangle = \left(\sum_{i=1}^{n} t_i \right) / n, \tag{3}$$

where t_i is the lifetime of guest-host hydrogen bond i in the trajectory, and n is the total number of guest-host hydrogen bonds (hits) formed in the trajectory. The average lifetime of the guest-host hydrogen bonds at 200 K is 0.28 ps. At the temperature of 250 K, in addition to the increasing probability of guest-host hydrogen bond formation (a greater number of hits), the average lifetime of the hydrogen bonds increases to 0.32 ps. An animation given in the supporting information shows the motion of the THF guests in the large sII cage at 200 K.[17]

At each snapshot of the trajectory, the ratio of the total number of guests with hydrogen bonds to the cage waters to the total number of guests in the simulation was binned. The average value of this ratio during the entire trajectory is used to determine the overall probability of guest-cage hydrogen bond formation at each temperature. This probability is related to the equilibrium constant of guest-host hydrogen bond formation. The van't Hoff plot of the logarithm of the probability of THF-cage hydrogen bond formation as a function of the inverse simulation temperature is plotted in Fig. 5. The plot for the THF sII clathrate gives a reaction enthalpy of ~8.2 kJ mol^{-1} for the guest-host hydrogen bond formation. This is the difference in energy between the water-THF and the water-water hydrogen bond in the clathrate.

At 150 K, the THP-water hydrogen bonds were found to be stable within the 200 ps simulation trajectory and the THP molecule is tethered by its oxygen end to a single OW atom. The animation in the supporting information[17] shows that the THP guests have small amplitude vibrations and the guest-host hydrogen bonds in the trajectory remain mostly intact. At 200 K, the THP guests detach from water molecules at regular time intervals and undergo partial rotation in the cage before forming new hydrogen bonds to a new cage water molecule.

The formation of guest-host hydrogen bonds and lattice defects in THF and THP clathrates drastically increases the range of water vibrational motions and cage deformations in the large cages. Additionally, long-lived *L*-type lattice defects affect the adjacent sII cages (both large and small) and can lead to structural correlations among guest positions in adjacent cages. The presence of lattice *L*-defects decreases the rotation barrier of nearby lattice water molecules and thus decreases the bulk activation barrier to dielectric relaxation in the clathrate phase.

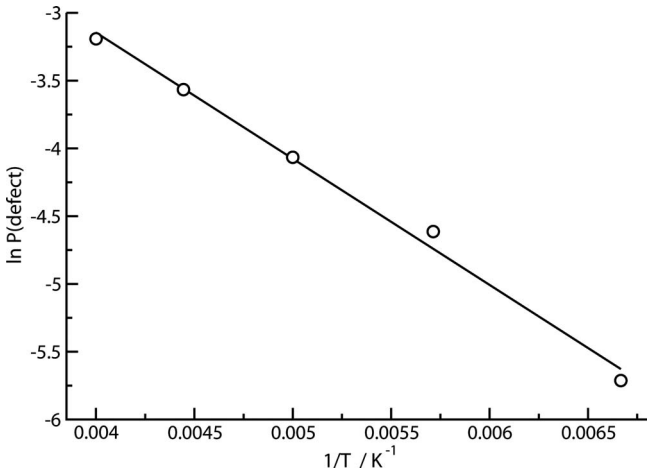

FIG. 5. The van't Hoff plot for the logarithm of the probability of the THF-water hydrogen bond formation as a function of the inverse temperature in the sII clathrate.

Hydroxide ions doped into ice phases lead to the formation of permanent *L*-defects in the water lattice analogous to the transient *L*-defects formed in THF and THP clathrates. A hydroxide ion introduces a *L*-defect in a neighboring hydrogen bond site which can diffuse away for the hydroxide ion.[29,30] It has been observed that OH^- doping catalyzes the transition of ice-I_h to ice-XI (Refs. 31–33) although the mechanism of the transition is not understood.[34–36] Proton ordering is also observed in the THF sII clathrate doped with KOH.[37] The K^+ cation is also known to play a role in the ordering process as it is more efficient than Na^+ in inducing proton ordering. Similar lattice transformations may be induced by long-lived guest-host hydrogen bonds in the clathrates.

In the time scale of our simulations we observe that despite having partial charges comparable to THF and THP and identical AMBER LJ parameters (see Table I), the ether oxygen atoms of 1,3-dioxolane and *p*-dioxane do not form hydrogen bonds with the cage water molecules. From our observations, three requirements must be met in order to form guest-host hydrogen bonds. First, the guest must have an electronegative hydrogen bond accepting atom. Second, the guest must have relatively large molecular volume (compared to the cage size) that places the electronegative atom in close proximity to the large cage water molecule. Third, the guest must have a large dipole vector that is oriented in the direction of an electronegative atom.

Of the five member ring molecules 1,3-dioxolane has the smallest molecular volume (see the figures for these molecules in the supporting information). As seen in Fig. 1, the first peaks in the OS-OW and OS-HW RDF curves for 1,3-dioxolane are spaced further out than those of the other

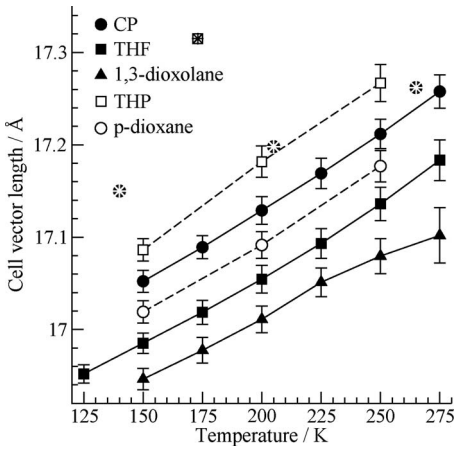

FIG. 6. Calculated temperature dependence of the lattice vector for CP, THF, 1,3-dioxolane, THP, and *p*-dioxane sII clathrates at ambient pressure. The magnitude of the lattice vector increases as the guest volumes become larger, but thermal expansivities of the clathrates are similar. Experimental data points for THF and THP clathrates are shown with the stars encased in circles and a square, respectively.

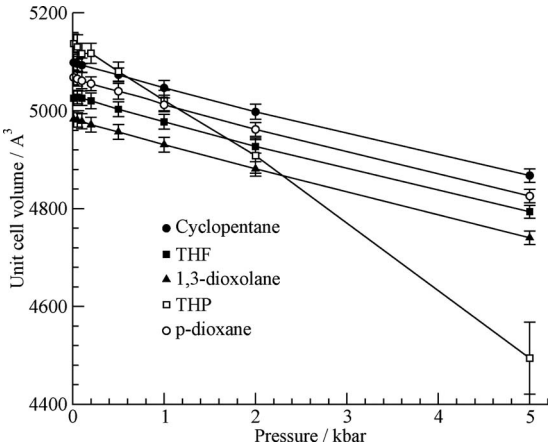

FIG. 7. Pressure dependence of unit cell volume for CP, THF, and 1,3-dioxolane, THP, and *p*-dioxane at 250 K.

guests (even CP) and this guest resides closer to the center of the large clathrate cages. There does not seem to be a strong interaction of the OS atoms in 1,3-dioxolane with water hydrogen atoms. The strong dipole moment of the 1,3-dioxolane molecule (1.71 D) is in the direction of the C2 atom and the net molecular electrostatic interactions are not directed toward either of the two ether oxygen atoms in this heterocyclic compound. Inspection of the cages in the simulation trajectory of 1,3-dioxolane also did not show the formation of guest-host hydrogen bonds.

The six-member *p*-dioxane molecule has a larger molecular volume than the five-member ring guests, but is smaller than the THP molecule (see supporting information). This molecule has a zero net dipole moment and so the molecule will not interact preferably with the cage water molecules in the direction of either ether oxygen atom. These factors could explain the observed absence of guest-host hydrogen bonding in simulations of the sII *p*-dioxane clathrate.

The larger volume of the THP molecule compared to the THF molecule can explain the fact that the guest-host hydrogen bonds in the THP clathrate are more stable and longer lived that the THF-water hydrogen bonds. This is discussed further below. An animation given in the Supporting Information shows the motion of the THP guests in the large sII cage at 150 K.

B. Volumetric properties

The temperature dependence of the lattice vector for the five cubic sII clathrate hydrates from 125 to 275 K at ambient pressure calculated are shown in Fig. 6. Experimental lattice vectors for THF and THP clathrates are also given for comparison.[38,39,3] The SPC/E-AMBER force field simulation underestimates the experimental unit cell vectors by ~2%. The lattice vectors generally increase according to the size of the guest molecules. For the guests with five-member rings, as the-CH_2 groups are substituted by O atoms in the sequence CP to THF to 1,3-dioxolane, the unit cell volume of the clathrate decreases. A decrease in the unit cell volume is also observed when comparing *p*-dioxane to THP sII clathrate. The effect of the guest molecule size dominates effects of the guest polarity on the unit cell volume of the clathrate. The thermal expansivity is related to the slope of Fig. 6 and is predicted to be similar for all clathrates studied in this work.

The pressure dependences of the unit cell volume for different sII clathrates at 250 K are shown in Fig. 7. The volumes of the CP, THF, 1,3-dioxolane, and *p*-dioxane sII clathrates vary linearly with the pressure and all have similar slopes. The isothermal compressibilities $\beta=-dV/VdP$ for these clathrates are given in Table II. At pressures higher than ~1 kbar, an inspection of the final simulation configurations shows that the THP sII clathrate is no longer mechanically stable (see figure in supporting information).[17] The mechanical instability of the THP clathrate may be related to the guest-host hydrogen bonding and lattice defect formation which diminishes the rigidity of the host water framework. This prediction of the instability of the THP clathrate should be experimentally verifiable.

C. Dynamic properties

The velocity autocorrelation functions (VACFs) of guests with five-member rings at 200 K and ambient pressure are shown in Fig. 8. The VACF is plotted at 0.05 ps intervals in these graphs. For THF, and 1,3-dioxolane the VACF of the OS atoms are plotted and for cyclopentane, the VACF of a carbon atoms is plotted. Despite the similar masses, cyclopentane has a shorter mean collision time (first *x*-intersect of the VACF) than the other two guest. The VACF of CP also decays to zero (randomizes) more rapidly (~1 ps) than

TABLE II. The isothermal compressibility ($kbar^{-1}$) of the sII clathrates at 250 K.

Guest	β
CP	0.009 09
THF	0.009 42
1,3-dioxolane	0.009 76
p-dioxane (200 K)	0.009 57

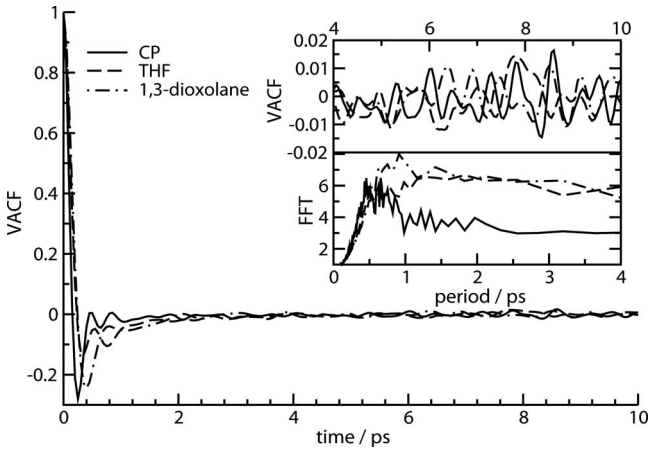

FIG. 8. The VACF for the chosen ring *X* atoms at 200 K and ambient pressure for CP, THF, and 1,3-dioxolane. The VACFs become randomized more quickly for CP. The inset shows the details of the oscillations in the VACF at long times. The fast Fourier transform (FFT) of the VACF shows the distribution of periods of the oscillations.

VACFs of THF or 1,3-dioxolane (~2 ps). The inset shows the magnified long-time behavior of the VACF for these guests along with the Fourier transforms of the VACFs plotted against the period of the oscillations. The time periods of the oscillations will give the frequencies that correlate roughly with the rattling frequencies of the clathrate IR spectrum and the ^{1}H NMR relaxation times at low temperatures for THF and cyclopentane.

The VACFs for THP and *p*-dioxane at 250 K and ambient pressure are shown in Fig. 9. The velocity randomization time for THP is <1 ps, which is shorter than the corresponding time for *p*-dioxane (~2 ps). The long-time behavior of the VACF and the Fourier transform of the VACF are shown in the inset. The VACFs of THP have somewhat smaller periods than those of *p*-dioxane.

The ensemble averages of the normalized guest orientational autocorrelation functions, $M(t)$ are shown in Fig. 10. For the polar THF and THP molecules, the orientational correlation functions are chosen to be identical to the normalized dipole-dipole autocorrelation function, $\langle \boldsymbol{\mu}(t)\cdot\boldsymbol{\mu}(0)\rangle/\langle \boldsymbol{\mu}(0)\cdot\boldsymbol{\mu}(0)\rangle$. For CP and *p*-dioxane, a unit vector in the direction connecting the center of mass of the molecule to a selected atom of the ring defines the orientation of the molecule. The orientational autocorrelation function $M(t)$ can be fit to a biexponential form,

$$M(t) = ae^{-t/\tau_1} + (1-a)e^{-t/\tau_2}, \tag{4}$$

with decay times τ_1 and τ_2. The values of the fit parameters are given in Table III.

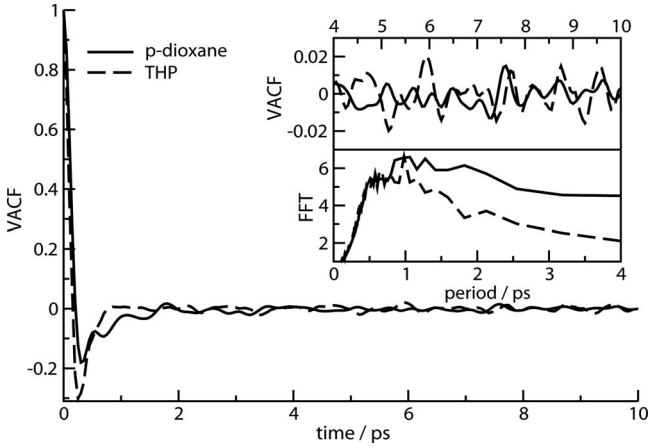

FIG. 9. The velocity autocorrelation function for the oxygen atoms for THP and *p*-dioxane at 200 K and ambient pressure. The inset shows the details of the oscillations in the VACF at long times and the FFT of the VACF curve.

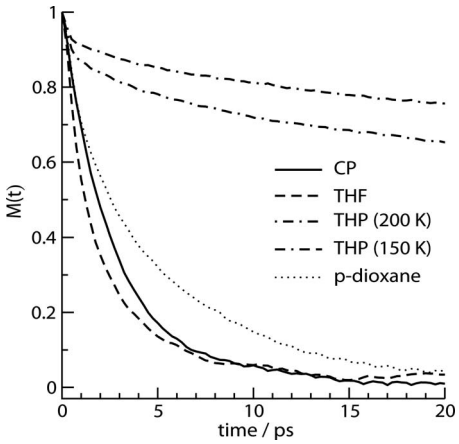

FIG. 10. The reduced orientational (dipole-dipole) autocorrelation functions for CP, THF, *p*-dioxane, and THP at 200 K and ambient pressure. The dipole-dipole autocorrelation function for THP at 150 K is also given.

In the five-member ring series, the orientational autocorrelation function of THF decays faster (τ_1=1.41 ps) than that of the larger CP molecule (τ_1=2.41 ps). The faster short-time decay of THF could be related to its smaller size. The $M(t)$ of THF in the sII large cages has a slower long-time decay than CP. The tethering and short-lived formation of hydrogen bonds of the THF molecules to the cage water oxygen atom, as seen in Figs. 2 and 4, may contribute to slower long-time decay of $M(t)$ for THF. The larger contribution of the long-time decay to the THF rotational dynamics is reflected in the smaller *a* parameter of Eq. (4) for THF. In contrast, the rotational motion of the larger CP is more continuous, giving rise to $M(t)$ which is close to a single exponential decay function.

The large six-member ring *p*-dioxane shows relatively slower decay of $M(t)$ than in the case of the five-member ring species, see Fig. 10. This is due to the more hindered motion of the larger *p*-dioxane molecules in the large sII clathrate cages. Of particular interest in Fig. 10 is the slow decay of the THP dipole-dipole correlation function at 150 and 200 K. In the 20 ps time frame of this figure, the THP molecules retain a strong memory of their original orienta-

TABLE III. Biexponential decay parameters for the orientational autocorrelation functions for guests in the sII large cages.

Guest	*a*	τ_1(ps)	τ_2(ps)
CP (200 K)	0.8787	2.41	8.15
THF (200 K)	0.7928	1.41	7.80
THP (150 K)	0.2391	6.65	549.6
THP (200 K)	0.3167	4.74	320.0
p-dioxane (200 K)	0.3312	1.20	6.67

TABLE IV. Experimental guest reorientation activation energies (kJ/mol), the guest-host defect formation activation energies, and the water reorientation energies for sII clathrates THF, CP, and *p*-dioxane. The water reorientation energy for hexagonal ice is given for comparison.

Guest	Guest reorientation E_{act}	Guest-host defect E_{act}	Water reorientation E_D
CP	2.67[a]	···	···
THF	3.80;[b] 3.84[a]	8.4	30.1;[a] 30.9[b]
1,3-dioxolane	3.80[b]	···	36.4
THP	···	···	···
p-dioxane	7.19;[c] 6.48[a]	···	38.0
I_h	···	···	56.5[d]

[a]From ^{1}H NMR relaxation-general reorientation.
[b]From dielectric dipole reorientation.
[c]From dielectric multipole reorientation.
[d]From Pines *et al.*, Ref. 40.

tion. The effect is even stronger at 150 K than at 200 K. When comparing the $M(t)$ of THP compared to *p*-dioxane, the slow decay cannot be solely attributed to larger guest volume of THP. The strong hydrogen bonding of the THP molecules with a single water molecule of the sII clathrate large cage effectively tethers it to this water site, which results in the retention of orientation for these guests in the cages and small *a* parameters. At 150 K the THP molecules remain predominantly hydrogen bonded to a single cage water molecule for the duration of the simulation, whereas at 200 K the THP molecules undergo attachment and detachment (followed by partial rotation) more frequently. This leads to a more rapid decay of the dipole-dipole correlation function at 200 K.

The results of our calculations for the guest-host hydrogen bonding and guest-induced lattice defect formation help to interpret experimental water dielectric relaxation times of different sII clathrate hydrates.[2] The THF guests form guest-host hydrogen bonds and the corresponding lattice defects. These lattice defects may induce further relaxation and rotational reorientation of the water molecules which will decrease the water dielectric relaxation time, τ_0, and dielectric relaxation activation energy, E_D, for this clathrate. On the other hand, 1,3-dioxolane and *p*-dioxane did not form guest-host hydrogen bonds in our simulations. The clathrates of these molecules have higher experimental water lattice dielectric relaxation times and activation energies, see Table IV. To our knowledge, data for THP dielectric relaxation have not been reported.

Our results are also consistent with the experimental trends observed for the activation energies of guest reorientations for the CP, THF, 1-3-dioxolane, and *p*-dioxane sII clathrates given in Table IV. The orientational autocorrelation functions shown in Fig. 10 were explained based on the sizes of the guest. The same trend explains the magnitudes of the activation energies of Table IV.

In this work, we have not explicitly studied the propagation of lattice defects in the water lattice or the correlations of defects and guest positions in the lattice during the simulation trajectories. Upon defect formation the water molecule hydrogen bonded to the guest still has four hydrogen bonds, but one of its neighbors in the cage will become undercoordinated. This is seen in Fig. 3 where the water molecule hydrogen bonded to the THP molecule has four hydrogen bonds. The *L*-defect is now in the second shell of water molecules from the guest hydrogen bonding site. In the case of the long-lived guest-host hydrogen bonds in the THP system, there is sufficient time for the water molecules to rotate and the lattice defects to propagate. This defect propagation enhances the dielectric relaxation in the clathrate water lattice. We see that the guest-host hydrogen bond formation activation energy in the THF clathrate corresponds roughly to the decrease in water reorientation activation energy in THF clathrate when compared to the 1-3-dioxolane and *p*-dioxane clathrates. In all cases, the water reorientation energies in the clathrates are less than the corresponding value in hexagonal ice.

IV. SUMMARY AND CONCLUSIONS

We have studied the sII clathrates with the cyclic guest molecules, cyclopentane, tetrahydrofuran, 1,3-dioxolane, tetrahydropyran, and *p*-dioxane. For each ring size (or equivalently in each isoelectronic series), the unit cell volume decreases as ring-CH_2-group are replaced by ether O atoms.

The ether oxygen atoms of the polar THF and THP molecules form guest-host hydrogen bonds with one sII large cage water molecule. These hydrogen bonds are accompanied by the formation of *L*-type Bjerrum defects in the clathrate lattice. The probability of guest-host hydrogen bond formation is relatively small in the THF clathrate and increases as the temperature of the clathrate is increased. This indicates that the guest-water hydrogen bond formation is a thermally activated process and is enhanced by the increased range of water lattice vibrations and guest rattling vibrations as the clathrate is heated. We obtain a reaction energy of roughly 8.3 kJ mol^{-1} for the formation of the guest-host hydrogen bonds in the THF clathrate. The guest size is larger in the THP clathrate and the closer contact of the ether oxygen atom in THP to the cage water molecule enhances the probability of guest-host hydrogen bonding in this clathrate. At temperatures as low as 150 K, strong guest-host hydrogen bonds are seen between THP and water which are stable up to a minimum of a few hundred picoseconds. At lower temperatures, the THP guest molecule remain tethered by an oxygen atom to the same cage water molecule, but as the THP sII clathrate is heated, the thermal vibrations lead to the breaking of the guest-host hydrogen bond. After a release of the guest, a partial rotation of the THP guest occurs and the THP will reform a new hydrogen bond with another cage water molecule. This leads to the quicker decay of the dipole-dipole correlation function of the THP guest molecules at higher temperatures as shown in Fig. 10. The presence of the stable guest hydrogen bonds in the THP clathrate is also observed in the RDF curves with water for this guest species that are shown in Fig. 1.

The lifetimes of the hydrogen bonds (and corresponding defects) in the THF clathrate are short. As temperature rises, in parallel to increasing probability of guest hydrogen bond formation, we observe greater occurrence of guest-water hydrogen bond formation, see Fig. 4.

The lattice defects caused by guest-water hydrogen bonding distort the clathrate lattice structures and may lead to more open cage faces in the clathrate. In binary THP and THF clathrates the distorted lattice structure may enhance the diffusion of small secondary guests, such as H_2 in the clathrate. This could have serious consequences for the capability of these clathrates for the long term storage of the secondary guest.[40]

Similar guest-host hydrogen bonding and lattice defects have been observed in computations of the sH *tert*-butylmethylether clathrate. The behavior of these systems is be described in another publication.[41]

ACKNOWLEDGMENTS

The support of the National Research Council of Canada was gratefully acknowledged.

[1] T. S. Yun, J. C. Santamarina, and C. Ruppel, J. Geophys. Res. B **112**, B04106 (2007); J. Kliner and J. Grozic, Can. Geotech. J. **43**, 551 (2006).
[2] D. W. Davidson and J. A. Ripmeester, in *Inclusion Compounds*, edited by J. L. Atwood, J. E. Davies, and D. D. MacNicol (Academic, New York, 1984), Vol. 3, p. 69.
[3] K. C. Hester, Z. Huo, A. L. Ballard, C. A. Koh, K. T. Miller, and E. D. Sloan, J. Phys. Chem. B **111**, 8830 (2007).
[4] S. Takeya, M. Kida, H. Minami, H. Sakagami, A. Hachikubo, N. Takahashi, H. Shoji, V. Soloviev, K. Wallmann, N. Biebow, A. Obzhirov, A. Salomatin, and J. Poort, Chem. Eng. Sci. **61**, 2670 (2006).
[5] E. D. Sloan, Jr., *Clathrate Hydrates of Natural Gases*, 2nd ed. (Dekker, New York, 1998).
[6] S. R. Gough, R. E. Hawkins, B. Morris, and D. W. Davidson, J. Phys. Chem. **77**, 2969 (1973).
[7] N. Bjerrum, Science **115**, 385 (1952).
[8] T. M. Kirschgen, M. D. Zeidler, B. Geil, and F. Fujara, Phys. Chem. Chem. Phys. **5**, 5247 (2003).
[9] S. K. Garg, D. W. Davidson, and J. A. Ripmeester, J. Magn. Reson. (1969-1992) **15**, 295 (1974).
[10] D. W. Davidson, S. K. Garg, and J. A. Ripmeester, J. Magn. Reson. **31**, 399 (1978).
[11] M. Bach-Vergés, S. J. Kitchin, K. D. M. Harris, M. Zugic, and C. A. Koh, J. Phys. Chem. B **105**, 2699 (2001).
[12] D. M. Jacobs, M. D. Zeidler, and O. Kanert, J. Phys. Chem. A **101**, 5241 (1997).
[13] T. R. Kessler and M. D. Zeidler, J. Mol. Liq. **129**, 39 (2006).
[14] A. Abragam, *The Principles of Nuclear Magnetism* (Oxford University Press, Oxford, 1961).
[15] T. C. Mak and R. K. McMullan, J. Chem. Phys. **42**, 2732 (1965).
[16] J. D. Bernal and R. H. Fowler, J. Chem. Phys. **1**, 515 (1933).
[17] See EPAPS Document No. E-JCPSA6-130-058917 for more details on the structure of the structure I clathrate hydrate and partial atomic charges on the atoms of the guest molecules used in the simulations. Animations of THF in a sample sI large cage and THP in a sample sI large cage are also given. For more information on EPAPS, see http://www.aip.org/pubservs/epaps.html.
[18] H. J. C. Berendsen, J. R. Grigera, and T. P. Straatsma, J. Phys. Chem. **91**, 6269 (1987).
[19] W. D. Cornell, P. Cieplak, C. L. Bayly, I. R. Gould, K. M. Merz, Jr., D. M. Ferguson, D. C. Spellmeyer, T. Fox, J. W. Caldwell, and P. A. Kollman, J. Am. Chem. Soc. **117**, 5179 (1995). Further i nformation on the AMBER force field can be found at http://amber.scripps.edu.
[20] C. M. Breneman and K. B. Wiberg, J. Comput. Chem. **11**, 361 (1990).
[21] M. J. Frisch, G. W. Trucks, H. B. Schlegel *et al.*, GAUSSIAN 98, Gaussian, Inc., Pittsburgh, PA, 2001.
[22] E. P. van Klaveren, J. P. J. Michels, J. A Schouten, D. D. Klug, and J. S. Tse, J. Chem. Phys. **114**, 5745 (2001); *ibid.* **115**, 10500 (2001); *ibid.* **117**, 6637 (2002).
[23] S. Alavi, J. A. Ripmeester, and D. D. Klug, J. Chem. Phys. **126**, 124708 (2007).
[24] *DL_POLY 2.16*, edited by T. R. Forester and W. Smith (CCLRC Daresbury Laboratory, Daresbury, UK, 2006).
[25] S. Nosé, J. Chem. Phys. **81**, 511 (1984); W. G. Hoover, Phys. Rev. A **31**, 1695 (1985); S. Melchionna, G. Ciccotti, and B. L. Holian, Mol. Phys. **78**, 533 (1993).
[26] D. Frenkel and B. Smit, *Understanding Molecular Simulation,* 2nd ed. (Academic, San Diego, 2000); M. P. Allen and D. J. Tildesley, *Computer Simulation of Liquids* (Oxford Science, Oxford, 1987).
[27] C. Vega, E. Sanz, and J. L. F. Abascal, J. Chem. Phys. **122**, 114507 (2005).
[28] G.-J. Guo, Y.-G. Zhang, and H. Lui, J. Phys. Chem. C **111**, 2595 (2007).
[29] H. Suga, T. Matsuo, and O. Yamamuro, Pure Appl. Chem. **64**, 17 (1992).
[30] C. Knight and S. J. Singer, in *Physics and Chemistry of Ice*, edited by W. F. Kuhs (RSC, Cambridge, 2007), p. 339.
[31] Y. Tajima, T. Matsuo, and H. Suga, Nature (London) **299**, 810 (1982).
[32] A. J. Leadbetter, R. C. Ward, J. W. Clark, P. A. Tucker, T. Matsuo, and H. Suga, J. Chem. Phys. **82**, 424 (1985).
[33] S. M. Jackson, V. M. Nield, R. W. Whitworth, M. Oguro, and C. C. Wilson, J. Phys. Chem. B **101**, 6142 (1997).
[34] M. J. Iedema, M. J. Dresser, D. L. Doering, J. B. Rowland, W. P. Hess, A. A. Tsekouras, and J. P. Cowin, J. Phys. Chem. B **102**, 9203 (1998).
[35] R. W. Whitworth, J. Phys. Chem. B **103**, 8192 (1999).
[36] J. P. Cowin and M. J. Iedema, J. Phys. Chem. B **103**, 8194 (1999).
[37] O. Yamamuro, T. Matsuo, and H. Suga, J. Inclusion Phenom. **8**, 33 (1990).
[38] C. Y. Jones, S. L. Marshall, B. C. Chakoumakos, C. J. Rawn, and Y. Ishii, J. Phys. Chem. B **107**, 6026 (2003).
[39] K. A. Udachin, C. I. Ratcliffe, and J. A. Ripmeester, J. Supramol. Chem. **2**, 405 (2002).
[40] A. Pines, E. D. Wemmer, D. J. Ruben, M. G. Usha, and R. J. Wittebort, J. Am. Chem. Soc. **110**, 5668 (1998).
[41] R. Susilo, S. Alavi, I. L. Moudrakovski, P. Englezos, and J. A. Ripmeester, ChemPhysChem **10**, 824 (2009).